The Astrophysical Journal, 576:860–869, 2002 September 10

MULTIWAVELENGTH OBSERVATIONS OF THE PECULIAR PLANETARY NEBULA IC 2149

R. Vázquez,[1] L. F. Miranda,[2] J. M. Torrelles,[3] L. Olguín,[4] G. Benítez,[1,5] L. F. Rodríguez,[6] and J. A. López[1]

Received 2001 August 18; accepted 2002 May 15

ABSTRACT

We report high- and low-dispersion spectroscopy, optical imaging, and high-resolution Very Large Array-A λ3.6 cm continuum observations of the peculiar planetary nebula IC 2149. These observations show that "bipolar" is a suitable morphological classification for IC 2149. Most nebular material is concentrated in a knotty, bright ring seen edge-on, embedded in an apparently oblate ellipsoidal shell from which remnant or incipient bipolar lobes emerge. We confirm the previously reported depletion in heavy elements and deduce a very low ejected nebular mass $\lesssim 0.03\ M_{\odot}$. All this information indicates that the formation of IC 2149 is the result of the evolution of a low-mass central star.

Subject headings: ISM: kinematics and dynamics — planetary nebulae: individual (IC 2149) — stars: AGB and post-AGB

1. INTRODUCTION

In the last 10 yr, the commonly accepted theory on formation of planetary nebulae (PNs), involving the interaction of stellar winds (Kwok, Purton, & Fitzgerald 1978), has been constantly revised in order to take into account a variety of morphologies, kinematics, and physical conditions recently found in PNs. Different scenarios, including equatorial density enhancements (Balick 1987), the evolution of binary systems forming accretion disks (Soker & Livio 1994), and the influence of stellar rotation and magnetized stellar winds (García-Segura 1997), have been proposed to explain the structures observed in PNs and, in particular, their basic morphological shapes as round, elliptical, and bipolar (Balick 1987). There are, however, some peculiar objects that have eluded a clear classification in terms of their morphological shapes.

IC 2149 is one of these peculiar PNs. It presents an elongated structure in narrowband optical images with two maxima: one coinciding with the central star, and the other at the northeastern extreme (Balick 1987). A similar structure has also been observed in radio continuum by Sistla & Kaftan-Kassim (1977). These authors show a λ3.6 cm map ($2\farcs8 \times 1\farcs8$ beam size) in which the two maxima observed at optical wavelengths can also be recognized. A faint envelope surrounds these bright structures. Using optical and UV spectra, Feibelman, Hyung, & Aller (1994) obtained an electron temperature of $T_e \simeq 10,000$ K and an electron density of $N_e \simeq 5600$ cm^{-3}, which are typical for PNs. Feibelman et al. (1994) also found depletion of heavy elements in the nebula. IC 2149 hosts a very bright central star ($V \simeq 11.34$, Ciardullo et al. 1999) with a stellar wind indicated by the presence of P Cygni profiles in the UV spectrum that indicate a wind velocity of $V_w \simeq 1000$–1600 km s^{-1} and a mass-loss rate of $\dot{M}_w \simeq 10^{-8}\ M_{\odot}$ yr^{-1} (Perinotto, Benvenuti, & Cerruti-Sola 1982; Feibelman et al. 1994). Recently, *Far Ultraviolet Spectroscopic Explorer* observations by Iping & Sonneborn (2002) indicate a beamed (possibly bipolar) mass outflow in IC 2149. Finally, Daub (1982) estimated a distance to IC 2149 of 1.1 kpc by means of statistical methods, which is consistent with the average of other individual estimates (Acker et al. 1992).

In this paper, we present radio and optical (ground- and space-based) data, including imaging and spectra of IC 2149. The main goal of this paper is to provide clues about the structure and formation of this peculiar PN.

2. OBSERVATIONS AND RESULTS

2.1. *CCD Narrowband Imagery*

Narrowband images of IC 2149 were obtained in 2000 October 18 at the 1.5 m telescope of the Observatorio de Sierra Nevada (OSN;[7] Granada, Spain). Filters in the emission lines of Hα ($\Delta\lambda = 10$ Å), [N II] λ6583 Å ($\Delta\lambda = 10$ Å), [O I] λ6300 Å ($\Delta\lambda = 50$ Å), [O III] λ5007 Å ($\Delta\lambda = 50$ Å), and [S II] λ6723 Å ($\Delta\lambda = 50$ Å) were used. The detector was a Thomson CCD with 1024×1024 pixels ($0\farcs33$ pixel^{-1} plate scale). Exposure time was 600 s in each image. Seeing was $\simeq 1\farcs5$ during the observations. The data were calibrated with the IRAF standard techniques for CCD direct images.

Figure 1 shows the images in Hα, [O III], [N II], [S II], and [O I]. In all the cases, emission is distributed in an elliptical envelope with the main axis oriented at P.A. $+67°$. Within this envelope, emission is stronger in a relatively narrow "band" along the main axis. The most conspicuous features in these images are the central star and the bright knot at the east side (hereafter EK, for "east knot"). In particular, EK dominates the emission in the Hα and [N II] images. The distance to EK from the central star varies with wave-

[1] Instituto de Astronomía, UNAM, Apartado Postal 877, Ensenada, BC 22800, Mexico; vazquez@astrosen.unam.mx, jal@astrosen.unam.mx, gbenitez@astrosen.unam.mx.

[2] Instituto de Astrofísica de Andalucía, CSIC, Apartado Postal 3004, E-18080 Granada, Spain; lfm@iaa.es.

[3] Institut d'Estudis Espacials de Catalunya (IEEC/CSIC) and Instituto de Ciencias del Espacio (CSIC), Edifici Nexus, c/Gran Capitá 2-4, 08034 Barcelona, Spain; torrelles@ieec.fcr.es.

[4] Instituto de Astronomía, UNAM, Apartado Postal 70-264, Mexico, DF 04510, Mexico; lorenzo@astroscu.unam.mx.

[5] Facultad de Ciencias, UABC, Apartado Postal 1880, Ensenada, BC 22800, Mexico.

[6] Instituto de Astronomía, UNAM, Apartado Postal 3-72 (Xangari), Mich, 58089 Morelia, Mexico; luisfr@astrosmo.unam.mx.

[7] The Observatorio de Sierra Nevada is operated by the Instituto de Astrofísica de Andalucía (CSIC) at Sierra Nevada (Granada, Spain).

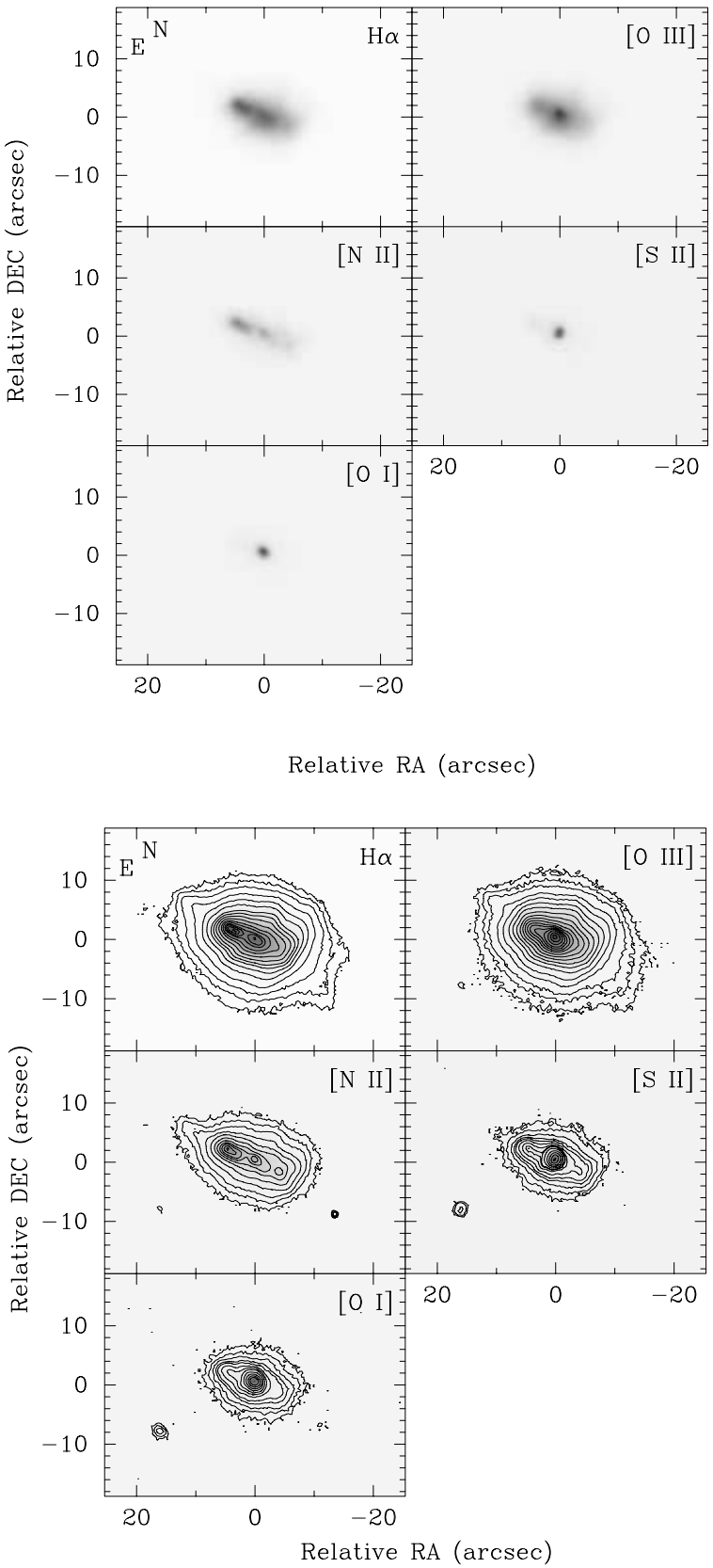

FIG. 1.—*Top*: Ground-based CCD images of IC 2149 obtained in several emission lines indicated in the top right corners. Gray levels were arbitrarily chosen. The origin, (0, 0), corresponds to the position of the central star. *Bottom*: As in top panel, but adding contours that were arbitrarily chosen in order to show the structure of both faint and bright nebular regions.

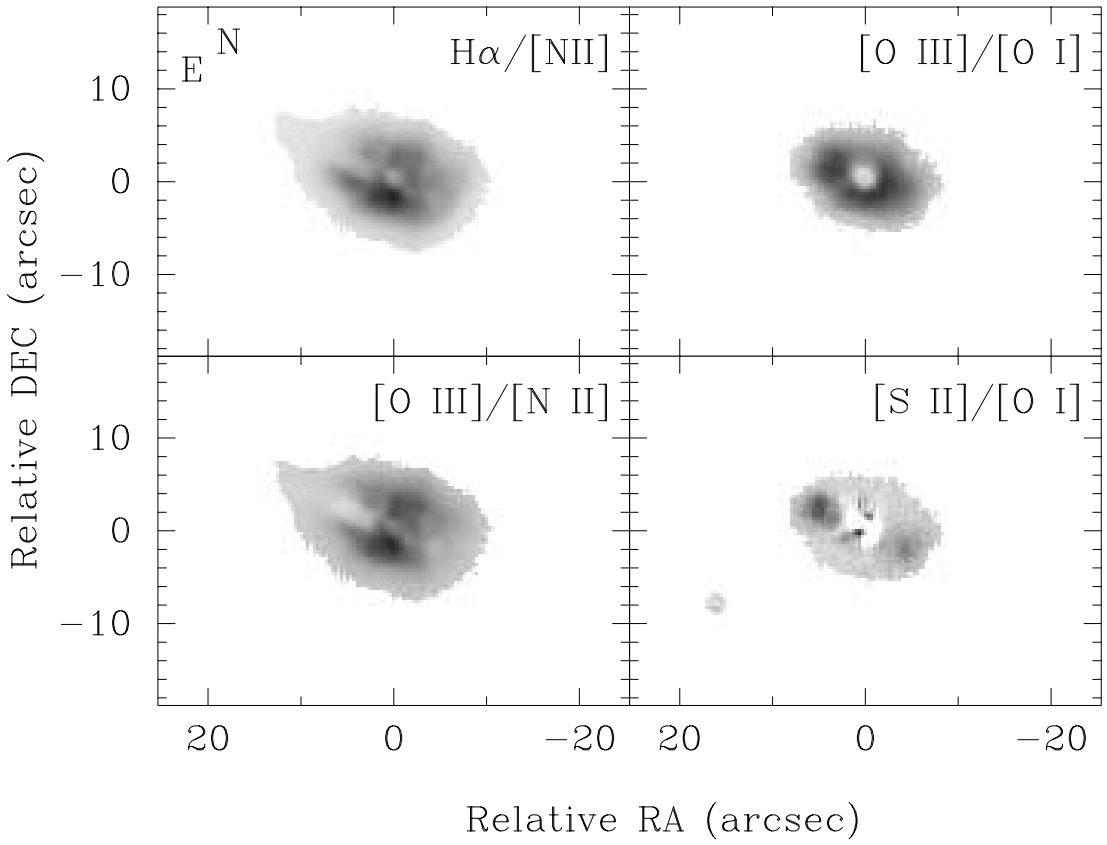

FIG. 2.—Intensity ratio images of IC 2149 based upon those shown in Fig. 1. White corresponds to lower values of the ratios.

length, having the following values: 3″.8 in Hα, 4″.7 in [N II], 3″.3 in [O III], 4″.7 in [S II], and 4″.3 in [O I]. A faint counterpart of EK toward the west (hereafter WK) can be clearly recognized in [N II] and [S II] and marginally observed in Hα, [O III], and [O I]. In addition, an extended structure is observed nearly perpendicular to the main nebular axis in Hα, [O III], and in [N II], and faint arclike extensions at the tips of the main nebular axis are recognizable in Hα, [O III], and partially in [N II].

Some image ratios are shown in Figure 2. These show that low-excitation emission is mainly concentrated within a central band along P.A. $+67^\circ$, whereas high-excitation emission is located in two extended regions outside this band. EK presents the lowest excitation in the nebula. Its counterpart, WK, can also be recognized in the ratio images as a low-excitation region.

2.2. *Radio Continuum* λ3.6 cm

The λ3.6 cm continuum observations were made with the Very Large Array (VLA) of the National Radio Astronomy Observatory (NRAO)[8] in the A configuration during 1996 December 23. The standard VLA continuum mode with a bandwidth of 100 MHz and two circular polarizations was employed. The absolute flux calibrator was 3C 286 (adopted flux density 5.18 Jy at λ3.6 cm), while 0555+398 was used as a phase calibrator (observed flux density 6.22 Jy at λ3.6 cm). The phase center was set at $\alpha(\mathrm{J2000.0}) = 05^{\mathrm{h}}56^{\mathrm{m}}23^{\mathrm{s}}.9$, $\delta(\mathrm{J2000.0}) = +46^\circ 06' 09''$. The on-target integration time was $\simeq$100 min. The data were calibrated using standard procedures of the AIPS package of the NRAO. Two cleaned maps were obtained by means of the task MX of AIPS. The first map was obtained with natural weighting of the (u, v) data, giving a synthesized beam $\simeq$0″.3 (rms noise $\simeq$8 μJy beam^{-1}). The second map was obtained using a Gaussian taper function of 400 kλ and restoring the data with a beam of 0″.6 (rms noise $\simeq$20 μJy beam^{-1}). The noise of the maps is consistent with the expected thermal noise. The measured total flux density at λ3.6 cm is $\simeq$50 mJy. This value is very different from that obtained by Sistla & Kaftan-Kassim (1977) ($\simeq$160 mJy) and could be due to the lower angular resolution used by these authors (more sensitive to weak and extended emission).

A contour/gray-scale mosaic of the two radio maps is shown in Figure 3. As in the optical images, the appearance of the nebula is elongated at P.A. $+67^\circ$, with the λ3.6 cm emission corresponding to the bright band observed in the optical images. In the map with a synthesized beam of 0″.6, at least six knots can be identified, with the EK and WK located at 4″.9 from the position of the central star. These knots apparently trace a very elongated ellipse with a size $\simeq 10'' \times 1''.2$. On the other hand, the higher resolution map, with a synthesized beam of 0″.3, provides the first view of the structure of the peculiar knot EK, whose appearance is reminiscent of a bow shock morphology.

[8] The National Radio Astronomy Observatory is a facility of the National Science Foundation operated under cooperative agreement by Associated Universities, Inc.

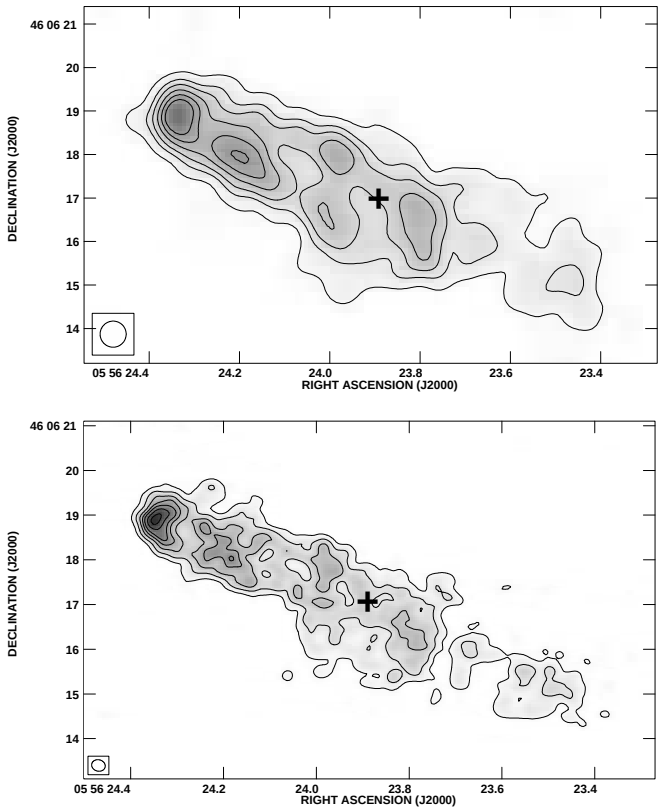

FIG. 3.—Shows $\lambda 3.6$ cm continuum gray-scale/contour maps of IC 2149. *Top*: Synthesized beam is $0\farcs6$. Contour levels are 10, 25, 40, 60, 80, and 100×20 μJy beam^{-1}, the rms of the map. *Bottom*: Synthesized beam is $\simeq 0\farcs3$. Contour levels are 5, 15, 30, 45, 60, and 80×8 μJy beam^{-1}, the rms of the map. In both maps, the position of the central star is indicated by the cross, corresponding to: $\alpha(\mathrm{J2000.0}) = 05^{\mathrm{h}}56^{\mathrm{m}}23^{\mathrm{s}}.9$, $\delta(\mathrm{J2000.0}) = 46^{\circ}06'17''$ (Gathier, Pottasch, & Goss 1986).

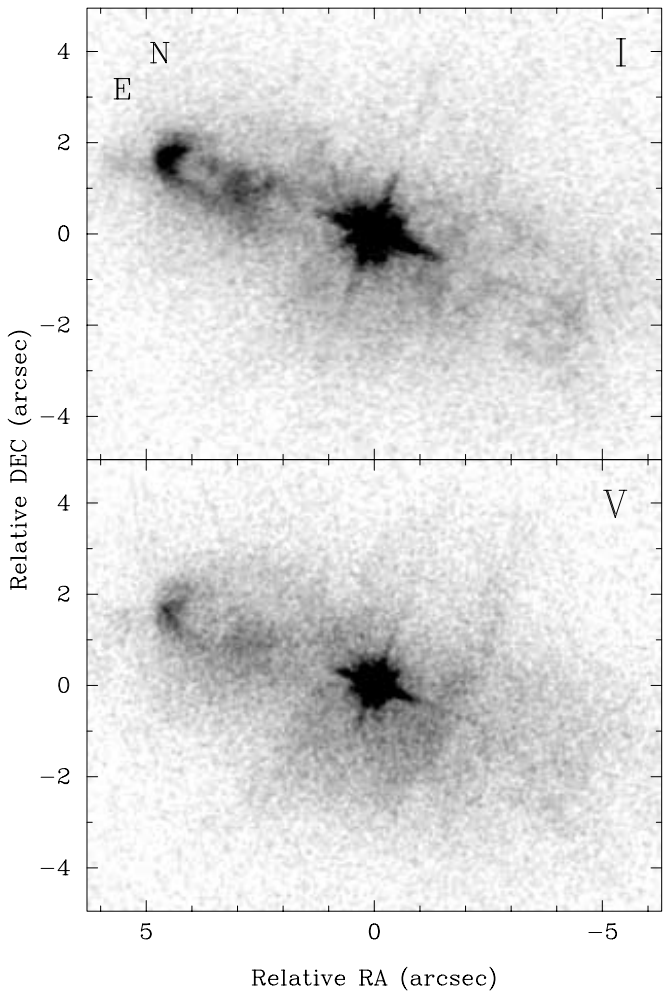

FIG. 4.—*HST*/WFPC2 images of IC 2149 taken with filters *I* (*top*) and *V* (*bottom*). A smoothing box (2×2 pixel) has been applied in order to increase the signal-to-noise ratio.

2.3. *Hubble Space Telescope Imagery*

In order to compare our VLA data with optical images at a similar spatial resolution, we have retrieved WFPC2 images from the *Hubble Space Telescope* (*HST*)[9] Archive (Proposal 6119, PI: H. Bond). We analyze processed images obtained in *V* (filter F555W, 7 s exposure time) and *I* (filter F814W, 2 s exposure time). The images shown in Figure 4 were smoothed with a 2×2 pixel box in order to increase the signal-to-noise ratio.

The brightest nebular feature is EK. The bow-shock–like structure identified in the radio continuum map (Fig. 3) can also be recognized in the *HST* images. WK is faint but definitely present in the *I* image. Other knots can also be observed that have a counterpart in the radio continuum map. We also note the presence of faint diffuse emission perpendicular to the main nebular axis, particularly in the *V* image. No further details about the internal structure of IC 2149 are revealed by the *HST* broadband images.

2.4. *High-Dispersion Long-Slit Spectroscopy*

High-dispersion long-slit spectra were obtained in 1998 August 2, with the IACUB[10] spectrograph at the 2.56 m Nordic Optical Telescope (NOT) at the Roque de los Muchachos Observatory (La Palma, Spain). A filter was used in order to isolate the Hα and [N II] λ6583 Å emission lines. A Thomson CCD with 1024×1024 pixels was used as a detector. Two spectra were obtained: one at P.A. $+67^{\circ}$, and one at P.A. -23°. In both cases, the exposure time was 900 s. The slit width was $0\farcs5$. The seeing was $\simeq 1\farcs3$ during the observations. The spectral resolution (FWHM of the comparison lines) was 0.17 Å (7.8 km s^{-1}). The data were reduced and calibrated using IRAF standard techniques for long-slit spectroscopy.

Figure 5 presents position-velocity (PV) maps of the Hα and [N II] λ6583 Å line profiles extracted from the two long-slit spectra. The Hα emission is more elongated at P.A. $+67^{\circ}$ ($\simeq 24''$) than at P.A. -23° ($\simeq 16''$), as observed in the direct images (Fig. 1). Extended Hα emission is observed toward the northeast and corresponds to the arclike extensions detected at the tips of IC 2149 in the direct images.

[9] This research was partially based on observations made with the NASA/ESA *Hubble Space Telescope*, obtained from the data archive at the Space Telescope Science Institute. STScI is operated by the Association of Universities for Research in Astronomy, Inc., under NASA contract NAS 5-26555.

[10] IACUB is a noncrossed dispersion echelle spectrograph, operated jointly by IAC and the University of Belfast.

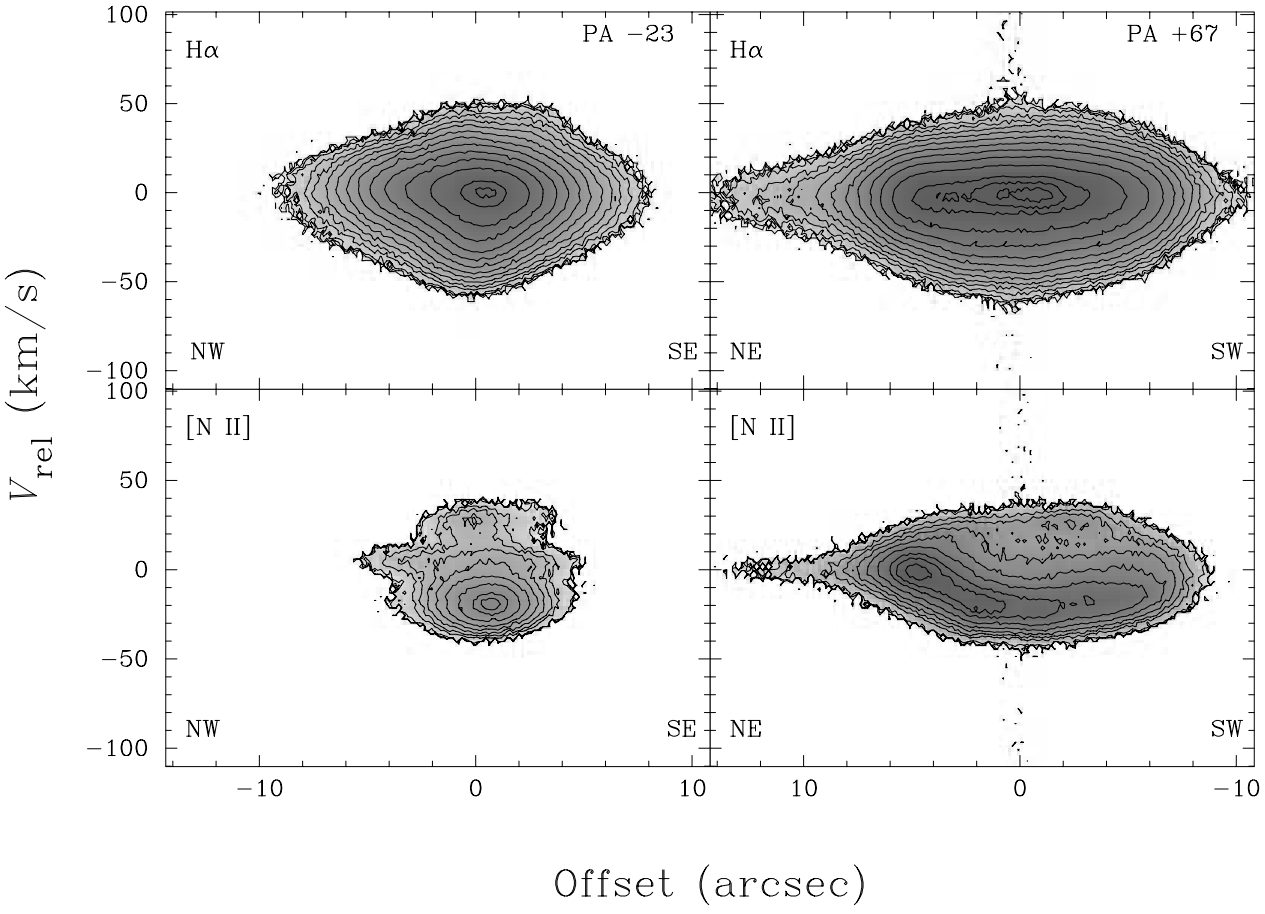

FIG. 5.—Position-velocity maps of the Hα (*top*) and [N II] λ6583 Å (*bottom*) emission lines obtained from the high-dispersion long-slit spectra of IC 2149 at position angles of −23° (*left*) and +67° (*right*). The gray levels and contours have been arbitrarily chosen in order to show the main features of the spectra. The origin, (0, 0), corresponds to the position of the central star (determined by the stellar continuum) and the systemic velocity of the nebula ($V_{LSR} = -38$ km s^{-1}), respectively.

The velocity width (FWHM) of the Hα emission line profile is ≈40 km s^{-1}, although the emission spreads at least ≈100 km s^{-1} at the level of 3 σ.

The PV maps of the [N II] λ6583 Å emission line shows many more details of the internal kinematics of IC 2149. At P.A. −23°, the [N II] emission is concentrated within ≃10″, and the PV map shows two components separated by ≃1″ along the slit and by ≃47 km s^{-1} in velocity (the blueshifted component displaced toward the southeast). The intensity of the blueshifted component is noticeably stronger than that of the redshifted. Additional emission is observed near the systemic velocity extending ≃10″. The PV map at P.A. +67° is rather different. An incomplete velocity ellipse is observed, with its blueshifted half stronger than its redshifted counterpart. The strongest emission, corresponding to EK, is observed in a compact region at ≃5″ northeast of the central star at the systemic velocity. The northeastern arc identified in the direct image (Fig. 1) can also be identified in the spectrum at P.A. +67° as faint, extended emission close to the systemic velocity, which we have determined as $V_{LSR} = -38 \pm 3$ km s^{-1}, comparable to the value of −33 km s^{-1} presented by Pottasch (1984).

2.5. *Low-Dispersion Long-Slit Spectroscopy*

Two low-dispersion spectra were obtained with a B&Ch spectrometer combined with the f/7.5 focus of the 2.1 m telescope at the Observatorio Astronómico Nacional (OAN-UNAM).[11] The first spectrum was obtained in 2000 January 14 using a 300 line mm^{-1} grating with a Tektronix CCD 1024 × 1024 (24 μm square pixels) as the detector, and a exposure time of 300 s. The observed wavelength interval is 3400–7500 Å, with 15 Å spectral resolution as measured from the FWHM of the HeAr comparison arc lines. This spectrum was used to measure the lower intensity lines along the spectral range.

The second spectrum was obtained in 2002 February 8 using a 600 line mm^{-1} grating with a SITe CCD 1024 × 1024 (24 μm square pixels) as the detector and an exposure time of 40 s. The observed wavelength interval is 4610–6700 Å, with 5 Å spectral resolution.

In both cases, a 150 μm (≡2.″0) slit width was used, with an orientation of P.A. +67°. The spectra were reduced and calibrated with the standard techniques of IRAF. Flux calibration was performed using sensitivity functions derived from observations of the standard stars Feige 34 and Hiltner 600.

Two one-dimensional spectra were extracted from each long-slit spectrum. These are shown in Figure 6, in which the top panel corresponds to EK and the bottom panel cor-

[11] The Observatorio Astronómico Nacional is operated by the Instituto de Astronomía (UNAM) at Sierra de San Pedro Mártir (Baja California, Mexico).

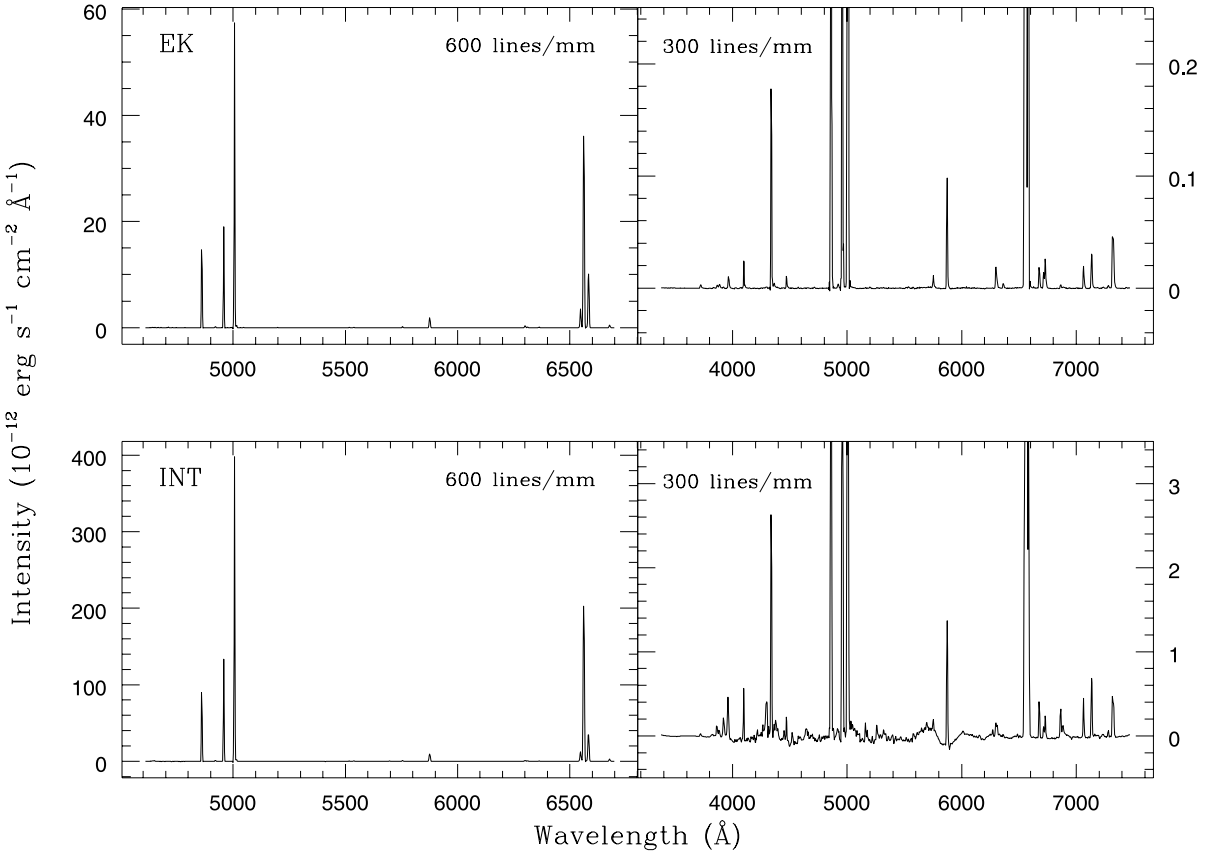

FIG. 6.—Low-dispersion spectra of IC 2149 co-added along the slit: EK (*top*) and INT (*bottom*). In both cases, the left box corresponds to the 600 line mm^{-1} grating and the right box to the 300 line mm^{-1} grating. Stellar continuum was fitted and removed.

responds to an integrated spectrum, hereafter denoted "INT spectrum." The EK spectra were obtained by adding the rows between 3″ and 6″ away from the central star on both long-slit spectra. The INT spectra were obtained by integrating the emission from each two-dimensional spectrum along the spatial direction (≃75″). In both panels, the left box corresponds to the 600 line mm^{-1} grating and the right box corresponds to the 300 line mm^{-1} grating; this last has been amplified in order to show the fainter emission lines. The stellar continuum has been subtracted from all the spectra.

According to Feibelman et al. (1994), the spectrum of the central star of IC 2149 contains hydrogen absorption in the Balmer lines. In such cases it is expected that, given the high intensity of the stellar emission, the presence of these absorption lines modifies the Hα/Hβ flux ratio in the nebula. In order to avoid using the $C_{\mathrm{H}\beta}$ coefficient derived from a spectrum that is contaminated with stellar photosphere, we obtained a Hα/Hβ flux ratio of the region from 7″ to 38″ from the central star toward the southwest, thus avoiding the stellar emission. The derived extinction coefficient was $C_{\mathrm{H}\beta} = 0.409$, which is consistent with that reported by Pottasch (1984) and the most recent value derived by Ciardullo et al. (1999) using *HST* flux-calibrated images.

The electron temperature and density, as well as ionic abundances by number, were estimated from the line fluxes using the abundance analysis software ALIEN (Cook & Vázquez 2002). The physical conditions and observed fluxes are shown in Table 1. The errors in the flux determination are ≈5%–10% for intense lines and ≈20%–30% for faint lines. The ionic abundances by number are shown in Table 2. The average values of ionic abundances were weighted with the fluxes of each line, giving less weight to the emission lines with lower signal-to-noise ratio. In addition, total elemental abundances were derived using the ionization correction factors (ICFs) from Kingsburgh & Barlow (1994) and are listed in Table 3.

Differences between our line fluxes, electron density and temperature, and abundances and those deduced by Feibelman et al. (1994) can be attributed to the different apertures used and uncertainties involved in the calculations, as well as the use of a different value for $C_{\mathrm{H}\beta}$.

On the other hand, our results confirm the depletion of heavy elements in the INT spectrum, as previously found by Feibelman et al. (1994). In the case of the EK spectrum, the O and Ne abundance is remarkably higher than the mean values for PNs and Type I PNs, whereas the S abundance is very similar to these mean values. There are also some differences in the electron temperature of both spectra ($\Delta T \simeq$ 1000–2000 K), whereas in both cases, the diagnostic line ratio for electron density is very close to the high-density limit. We also note that enhanced low-excitation emissions are not observed in EK, and further indications of shock excitation are not observed in the spectra.

3. DISCUSSION

3.1. *The Geometric and Kinematic Structure of IC 2149*

If only the optical and radio images are considered, IC 2149 could be classified as an elliptical PN whose major axis

TABLE 1
OBSERVED (F) AND DEREDDENED (I) RELATIVE FLUXES OBTAINED FOR THE EK AND INT SPECTRA AND THEIR DERIVED PHYSICAL CONDITIONS

Ion	λ_0 (Å)	f_λ	F(EK)	F(INT)	I(EK)	I(INT)
[O II]	3727	0.258	0.9	0.6	1.1	0.8
[Ne III]	3868	0.231	0.6	1.8	0.7	2.3
H8	3889	0.228	1.0	1.7	1.3	2.1
[Ne III]	3969	0.212	2.0	8.9	2.4	10.9
Hδ	4101	0.183	3.6	7.3	4.3	8.7
Hγ	4340	0.127	24.6	35.2	27.7	39.6
[O III]	4363	0.122	0.7	2.1	0.7	2.4
He I	4471	0.096	1.8	3.2	2.0	3.5
Hβ	4861	0.000	100	100	100	100
He I	4921	−0.016	1.4	1.5	1.4	1.5
[O III]	4959	−0.023	120.2	156.5	117.6	153.0
[O III]	5007	−0.036	353.6	455.9	341.8	440.7
[N II]	5755	−0.194	2.2	1.3	1.8	1.1
He I	5876	−0.214	17.1	16.8	14.0	13.7
[O I]	6300	−0.281	3.4	1.5	2.6	1.2
[S III]	6312	−0.283	1.2	0.9	0.9	0.7
[O I]	6364	−0.291	1.3	0.5	1.0	0.4
[N II]	6548	−0.318	33.6	19.2	24.9	14.3
Hα	6563	−0.321	342.8	358.8	253.6	265.5
[N II]	6583	−0.323	100.1	62.1	73.9	45.8
He I	6678	−0.336	3.2	4.6	2.4	3.4
[S II]	6717	−0.341	2.1	2.0	1.5	1.5
[S II]	6731	−0.343	5.2	4.1	3.8	2.9
He I	7065	−0.387	3.7	6.7	2.6	4.6
[Ar III]	7135	−0.396	6.0	10.9	4.2	7.5
[O II]	7327	−0.419	15.2	5.6	10.2	3.8
log $F_{\mathrm{H}\beta}$	...	...	−10.30	−9.44	...	...
log $I_{\mathrm{H}\beta}$	...	...	...	...	−9.89	−9.03
N_e([S II]) (cm^{-3})	...	...	...	...	10000	9600
T_e([O III]) (K)	...	...	...	...	7400	9400
T_e([N II]) (K)	...	...	...	...	11000	10000

NOTE.—The units of $F_{\mathrm{H}\beta}$ and $I_{\mathrm{H}\beta}$ are ergs s^{-1} cm^{-2}. The spectra were dereddened using the Seaton 1979 Galactic extinction law (f_λ).

is oriented at P.A. +67° (Fig. 3), containing a highly collimated bipolar outflow defined by a bow shock (EK) with a weaker counterpart called the "west knot" (WK). In some respects, the images of IC 2149 resemble the *HST* Near-Infrared Camera and Multi-Object Spectrometer (NICMOS) image of the Egg Nebula (Sahai et al. 1998), although in IC 2149 no "torus" perpendicular to the apparent ejecta and no waist between them are observed. Furthermore, our additional data do not support this scenario. EK does not exhibit the large velocity widths and the stratification expected from bow shock excitation. In fact, no evidence for shock excitation in EK has been found. The velocity ellipse observed at P.A. +67° would be compatible with an ellipsoidal shell, but the expected velocity ellipse at P.A. −23° is not observed. Moreover, the inner layers are of low excitation and are surrounded by layers of high excitation (Fig. 2), which would represent a very unusual stratification for an elliptical PN.

Despite the peculiar morphology in the images, the long-slit spectra provide very valuable information to deduce the basic structure of IC 2149. The PV maps of the [N II] line are those expected from a ringlike, inhomogeneous structure observed nearly edge-on with the axis oriented at P.A. −23°. The long-slit spectrum at P.A. +67° covers the whole ring, and the observed velocity ellipse corresponds to the two halves of the ring. At P.A. −23°, the slit intersects small portions of the ring located along the line of sight to the central star, which appear as two velocity components in the PV map. In this geometry, the extreme regions of the ring, corresponding to EK and WK, are brighter as expected from a higher density effect, and the bow shock shape of EK is a consequence of the curved end of the ring. Assuming that the ring is circular, the PV maps indicate an inclination of the ring axis of $\simeq$86° with respect to the line of sight (with the southeast half of the ring approaching the observer). An identical value for the inclination is deduced from the ellipse that can be fitted to the radio continuum (Fig. 2, *top panel*), which represents the best view of the edge-on ring. The expansion velocity of the ring is $\simeq$24 km s^{-1}, which, combined with a radius of $\simeq$5″ and a distance of 1.1 kpc, yields a kinematic age of $\simeq$1100 yr for the ring.

The Hα and [O III] images and the long-slit spectra indicate that the ring is embedded in an elliptical shell. Given that this shell shares the orientation of the ring, it indicates an oblate ellipsoidal geometry. In addition, the arclike structures at the extremes of the ring suggest the possible presence of faint bipolar lobes, which are responsible for the faint extended emission observed in the PV maps of Hα and [N II] (see also the Digitized Sky Survey images in the *HST* Archive, in which the arclike structures are evident, as well as an apparent halo). These results indicate that IC 2149 can be classified as a bipolar PN with a "diabolo" geometry

TABLE 2
IONIC ABUNDANCES BY NUMBER FOR THE EK AND INT SPECTRA

Ion	λ_0 (Å)	EK Spectrum	INT Spectrum
He^+.....	4471	3.500×10^{-2}	6.700×10^{-2}
	5876	1.080×10^{-1}	9.000×10^{-2}
	6678	7.900×10^{-2}	8.200×10^{-2}
	Average	9.777×10^{-2}	8.600×10^{-2}
Ne^{2+} ...	3868	2.954×10^{-6}	2.965×10^{-6}
	3969	3.195×10^{-5}	4.592×10^{-5}
	Average	2.537×10^{-5}	3.861×10^{-5}
Ar^{2+}....	7135	7.691×10^{-7}	7.239×10^{-7}
O^{2+}	4363	4.045×10^{-4}	1.956×10^{-4}
	4959	3.979×10^{-4}	1.997×10^{-4}
	5007	4.018×10^{-4}	1.998×10^{-4}
	Average	4.008×10^{-4}	1.997×10^{-4}
O^+.....	3727	2.298×10^{-6}	9.891×10^{-7}
	7327	2.860×10^{-4}	1.811×10^{-4}
	Average	2.707×10^{-4}	1.639×10^{-4}
O^0	6300	3.721×10^{-6}	2.301×10^{-6}
	6364	4.437×10^{-6}	2.507×10^{-6}
	Average	3.920×10^{-6}	2.355×10^{-6}
N^+	5755	1.227×10^{-5}	1.156×10^{-5}
	6548	1.224×10^{-5}	8.932×10^{-6}
	6584	1.232×10^{-5}	9.747×10^{-6}
	Average	1.230×10^{-5}	9.586×10^{-6}
S^{2+}	6312	8.676×10^{-6}	1.988×10^{-6}
S^+	6717	2.303×10^{-7}	2.800×10^{-7}
	6731	2.860×10^{-7}	2.778×10^{-7}
	Average	2.700×10^{-7}	2.785×10^{-7}

(see Monteiro et al. 2000), whose main axis (bipolar axis) is oriented along P.A. $-23°$. Figure 7 shows a schematic representation of the nebula and its structures. This result is in agreement with Feibelman et al. (1994), who suggest that IC 2149 consists of a bright, dense torus and two faint polar cones, and with Zhang & Kwok (1998), who model IC 2149 as a bipolar PN.

The geometric structure of IC 2149 is very similar to that observed in A79 (Balick 1987) and He 2-428 (Manchado et al. 1996), the difference between the three PNs being probably their orientation with respect to the observer. In all these PNs, a distorted and/or inhomogeneous ring is the brightest structure from which faint, asymmetric arcs emerge denoting the presence of bipolar lobes. IC 2149 is also similar to SuWt 2 and WeBo 1 , other cases of ring nebulae that are considered bipolar (Exter, Bond, & Pollaco 2002).

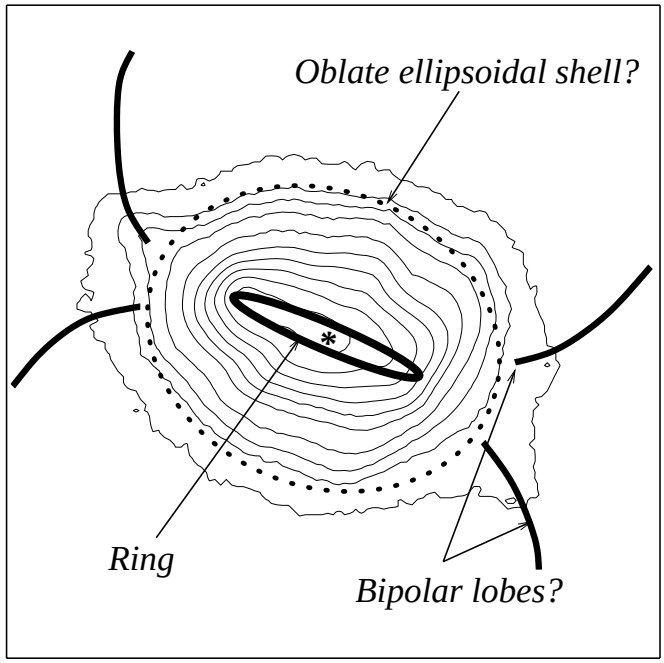

FIG. 7.—Schematic representation of IC 2149. The main brightest and densest structure is a ring seen almost edge-on. A possibly oblate ellipsoidal shell surrounds the ring, and incipient or remnant bipolar lobes are observed and indicated. According to the data, IC 2149 may be classified as a bipolar PN (diabolo type) with the main axis at P.A. $-23°$.

3.2. *The Formation of IC 2149*

The highly inhomogeneous structure suggests that IC 2149 is an evolved PN. However, the nebula is rather compact; its kinematic age is relatively small (although if the shell has been recently accelerated, the kinematic age would be larger); and the electron density (Table 1) is relatively high, more in accord with a young PN. However, no evidence for noticeable amounts of neutral or molecular material has been found in IC 2149 [$M(\mathrm{H\ I}) < 0.4M(\mathrm{H\ II})$, Schneider et al. 1987; $M(\mathrm{CO}) < 1.5 \times 10^{-3}\ M_\odot$, Huggins & Healy 1989; see also Dinerstein, Sneden, & Uglum 1995 and Hora, Latter, & Deutsch 1999], as would be expected in a young PN.

TABLE 3
COMPARISON OF THE TOTAL ELEMENTAL ABUNDANCES

Abundance	ICF(EK)	ICF(INT)	EK	INT	F94[a]	PNs[b]	TI PNs[c]	H II[d]	Sun[e]
He/H.....	...	...	0.10 ± 0.03	0.09 ± 0.04	0.09	0.12 ± 0.02	0.13 ± 0.04	0.10 ± 0.01	0.10 ± 0.01
O/H.....	1.00	1.00	8.83 ± 0.04	8.56 ± 0.04	8.46	8.68 ± 0.15	8.65 ± 0.15	8.70 ± 0.04	8.93 ± 0.04
N/H.....	2.48	2.22	7.48 ± 0.08	7.33 ± 0.08	8.69	8.35 ± 0.25	8.72 ± 0.15	7.57 ± 0.04	8.00 ± 0.04
Ne/H.....	1.68	1.82	8.83 ± 0.26	7.85 ± 0.26	7.43	8.09 ± 0.15	8.09 ± 0.15	7.90 ± 0.10	8.09 ± 0.10
Ar/H	1.87	1.87	6.16 ± 0.26	6.13 ± 0.26	5.90	6.39 ± 0.30	6.42 ± 0.30	6.42 ± 0.04	6.56 ± 0.10
S/H.....	1.08	1.06	6.99 ± 0.13	6.38 ± 0.13	6.62	6.92 ± 0.30	6.91 ± 0.30	7.06 ± 0.06	7.21 ± 0.06
N/O.....	...	...	0.05 ± 0.01	0.06 ± 0.03	0.17	0.47 ± 0.30	1.17 ± 0.60	0.07 ± 0.02	0.13 ± 0.02

NOTE.—Except for He, all the abundances relative to H are logarithmic values with $\log \mathrm{H} = +12$.
[a] Taken from Feibelman et al. 1994.
[b] Average for PNs (Kingsburgh & Barlow 1994).
[c] Average for Type I PNs (Kingsburgh & Barlow 1994).
[d] Average for H II regions (Shaver et al. 1983).
[e] The Sun (Grevesse & Anders 1989).

Given that shaping of PNs has a dependence on the properties of the central star (Mellema 1997), it is of interest to analyze the characteristics of the central star of IC 2149.

The low effective temperature ($T_{\rm eff} \simeq 30$–40×10^3 K) and the detection of a stellar wind suggest an early evolutionary stage of the central star. Herrero, Méndez, & Manchado (1990) obtained a stellar mass of $\simeq 0.73\ M_\odot$, implying a massive progenitor. This corresponds to an evolutionary age ≤ 200 yr (Blöcker 1995), which is compatible with a recently formed PN. However, a massive progenitor would have ejected a massive envelope, and it is highly improbable that all ejected material has been ionized during the very short lifetime of the central star. Furthermore, the depletion of heavy elements in the nebula is incompatible with a massive progenitor. In fact, these two observational results (no noticeable neutral or molecular material and depletion of heavy elements) indicate that the mass of the central star is less than $0.73\ M_\odot$ (see Feibelman et al. 1994). If we assume a lower stellar mass of, say, $\sim 0.55\ M_\odot$ (corresponding to a progenitor of $\sim 1\ M_\odot$), the relatively low $T_{\rm eff}$ and presence of a stellar wind would be a result of the very slow evolution of the central star with an evolutionary age of a several thousand years, rather than indicating a very young central star. A low-mass progenitor is compatible with the depletion of heavy elements. In addition, the mass of the ejected envelope is expected to be small and would be fully ionized during the long evolutionary time.

A critical test in the low-mass central star hypothesis is the mass of the envelope. In order to obtain an estimate, we assume a sphere of radius $5''$ with uniform electron density at a distance of 1.1 kpc. With these parameters, the radio continuum flux at $\lambda 3.6$ cm, and the formulation of Mezger & Henderson (1967), we obtain a value for the ionized nebular mass of $M(\mathrm{H\ II}) \simeq 0.01\ M_\odot$. If we use the electron density deduced from the optical spectrum (Table 1) and the same geometry, we find $M(\mathrm{H\ II}) \simeq 0.02\ M_\odot$. This value should be considered as an upper limit to the actual ionized nebular mass because the assumed electron density pertains to the dense ring, whereas it is much lower in the rest of the sphere. Thus, a substantial filling factor would have to be considered in this estimate. Taking into account that the amount of neutral or molecular material is at the limit of detection (less than $0.01\ M_\odot$; see references above), the value deduced for the total mass ejected by the progenitor of the central star can be considered to be $M \lesssim 0.03\ M_\odot$. This very small value deduced for the ejected mass supports the hypothesis of a low-mass central star.

Models for the evolution of low-mass central stars of PN suggest that when the star evolves slowly, any anisotropic density distribution in the envelope is smoothed out (Mellema 1997). This is not the case for IC 2149, in which anisotropies in the envelope have persisted for several thousand years. The fragmented structure of the nebula could indicate that anisotropies in the envelope are disappearing. However, the presence of an ellipsoidal shell suggests that the nebula may still be in the process of forming and that complete bipolar lobes could be developed in the future. The fact that low-mass central stars are capable of developing into nonspherical PNs, in contradiction with theoretical expectations, has already been recognized in NGC 4361 (Vázquez et al. 1999). Some similarities can be noted between IC 2149 and NGC 4361. Both PNs present very small nebular masses and the depletion of heavy elements, which are consistent with a low-mass progenitor. An equatorial ring and bipolar lobes are observed in both PNs, although in different stage of development. In IC 2149, the ring is more prominent than the lobes, whereas the contrary is true for NGC 4361. The central star of NGC 4361 is considerably hotter than the central star of IC 2149 (Méndez et al. 1988). Attending to these comparisons, it is not unlikely that these two PNs correspond to different phases of the final evolution of low-mass central stars, NGC 4361 being the more evolved.

4. CONCLUSIONS

A set of observational data of the peculiar PN IC 2149 is presented, including optical ground- and space-based images, radio continuum VLA images, and high- and low-dispersion spectra. Although the nebula appears as an elliptical PN with highly collimated outflows, a detailed analysis of the data indicate that it consists of a bright inhomogeneous ring, embedded in an oblate ellipsoidal shell, from which traces of bipolar lobes emerge. We conclude that the most suitable classification for IC 2149 is that of a bipolar PN with a diabolo geometry. The previously reported underabundance of heavy elements in the nebula is confirmed by our data. In addition, a very low nebular mass ($\leq 0.03\ M_\odot$) is inferred. The properties of IC 2149 can be understood if the formation of the nebula is related to a low-mass central star.

This work has been partially supported by the Programa de Cooperación Científica con Iberoamérica. R. V. was supported by CONACYT grant I32812-E and DGAPA-UNAM grant IN114199 (Mexico). L. F. M. and J. M. T. were partially supported by DGESIC grant PB98-0670-C02 and by Junta de Andalucía (Spain). J. A. L. and L. F. R. acknowledge continuous support from DGAPA-UNAM (Mexico) and CONACYT (Mexico). L. O. is in grateful receipt of a graduate scholarship from DGEP-UNAM (Mexico). The Nordic Optical Telescope is operated on the island of La Palma jointly by Denmark, Finland, Iceland, Norway, and Sweden, in the Spanish Observatorio del Roque de los Muchachos of the Instituto de Astrofísica de Canarias. We thank the staff of all the facilities used (OSN, VLA, *HST* Archive, NOT, and SPM) for their excellent assistance during the data acquisition. We acknowledge S. Zharikov, G. Tovmassian, A. Moitinho, and M. Richer for useful discussions, and to the anonymous referee for valuable comments that have improved the original manuscript.

REFERENCES

Acker, A., Ochsenbein, F., Stenholm, B., Tylenda, R., Marcout, J., & Schohn, C. 1992, Strasbourg-ESO Catalogue of Galactic Planetary Nebulae (Münich: ESO)
Balick, B. 1987, AJ, 94, 671
Blöcker, T. 1995, A&A, 299, 755
Ciardullo, R., Bond, H. E., Sipior, M. S., Fullton, L. K., Zhang, C.-Y., & Schaefer, K. G. 1999, AJ, 118, 488
Cook, R., & Vázquez, R. 2002, Rev. Mexicana Astron. Astrofis. Ser. Conf., 12, 38
Daub, C. T. 1982, ApJ, 260, 612
Dinerstein, H. L., Sneden, C., & Uglum, J. 1995, ApJ, 447, 262
Exter, K., Bond, H. E., & Pollaco, D. L. 2002, in IAU Symp. 209, Planetary Nebulae: Their Evolution and Role in the Universe, in press
Feibelman, W. A., Hyung, S., & Aller, L. H. 1994, ApJ, 426, 653

García-Segura, G. 1997, ApJ, 489, L189
Gathier, R., Pottasch, S. R., & Goss, W. M. 1986, A&A, 157, 191
Grevesse, N., & Anders, E. 1989 in AIP Conf. Proc. 183, Cosmic Abundances of Matter, ed. C. J. Waddington (New York: AIP), 1
Herrero, A., Méndez, R. H., & Manchado, A. 1990, Ap&SS, 169, 183
Hora, J. L., Latter, W. B., & Deutsch, L. K. 1999, ApJS, 124, 195
Huggins, P. J., & Healy, A. P. 1989, ApJ, 346, 201
Iping, R. C., & Sonneborn, G. 2002, in IAU Symp. 209, Planetary Nebulae: Their Evolution and Role in the Universe, in press
Kingsburgh, R. L., & Barlow, M. J. 1994, MNRAS, 271, 257
Kwok, S., Purton, C. R., & Fitzgerald, P. M. 1978, ApJ, 219, L125
Manchado, A., Guerrero, M. A., Stanghellini, L., & Serra-Ricart, M. 1996, The IAC Morphological Catalog of Northern Galactic Planetary Nebulae (La Laguna: IAC)
Mellema, G. 1997, A&A, 321, L29
Méndez, R. H., Kudritzki, R. P., Herrero, A., Husfeld, D., & Groth, H. G. 1988, A&A, 190, 113
Mezger, P. G., & Henderson, A. P. 1967, ApJ, 147, 471
Monteiro, H., Morisset, C., Gruenwald, R., & Viegas, S. M. 2000, ApJ, 537, 853
Perinotto, M., Benvenuti, P., & Cerruti-Sola, M. 1982, A&A, 108, 314
Pottasch, S. R. 1984, Planetary Nebulae (Dordrecht: Reidel)
Sahai, R., Hines, D. C., Kastner, J. H., Weintraub, D. A., Trauger, J. T., Rieke, M. J., Thompson, R. I., & Schneider, G. 1998, ApJ, 492, L163
Schneider, S. E., Silvergate, P. R., Altshuler, D. R., & Giovanardi, C. 1987, ApJ, 314, 572
Seaton, M. J. 1979, MNRAS, 187, P73
Shaver, P. A., McGee, R. X., Newton, L. M., Danks, A. C., & Pottasch, S. R. 1983, MNRAS, 204, 53
Sistla, G., & Kaftan-Kassim, M. A. 1977, MNRAS, 178, 325
Soker, N., & Livio, M. 1994, ApJ, 421, 219
Vázquez, R., López, J. A., Miranda, L. F., Torrelles, J. M., & Meaburn, J. 1999, MNRAS, 308, 939
Zhang, C. Y., & Kwok, S. 1998, ApJS, 117, 341